

This is a peer-reviewed, accepted author manuscript of the following research article:  
Warzecha, M, Yerragunta, M, Florence, AJ & Vekilov, PG 2025, 'Modifiers regulate crystal morphology by generating lattice defects', *Crystal Growth and Design*.  
<https://doi.org/10.1021/acs.cgd.5c01526>

## **Modifiers regulate crystal morphology by generating lattice defects**

Monika Warzecha,<sup>1,2</sup> Manasa Yerragunta,<sup>3,4</sup> Alastair J. Florence,<sup>1,2</sup> Peter G. Vekilov<sup>3,4,5,\*</sup>

<sup>1</sup> *Strathclyde Institute of Pharmacy and Biomedical Sciences, University of Strathclyde, 161 Cathedral Street, Glasgow, G4 0RE, UK*

<sup>2</sup> *EPSRC Future Continuous Manufacturing and Advanced Crystallization Research Hub, University of Strathclyde, Technology and Innovation Centre, 99 George Street, Glasgow, G1 1RD, U.K.*

<sup>3</sup> *William A. Brookshire Department of Chemical and Biomolecular Engineering, 4226 Martin L. King Blvd., University of Houston, Houston, Texas 77204-4004, USA*

<sup>4</sup> *Welch Center for Advanced Bioactive Materials Crystallization, University of Houston, 4226 Martin L. King Blvd., Houston, Texas 77204-4004, USA*

<sup>5</sup> *Department of Chemistry, University of Houston, 3585 Cullen Blvd., Houston, Texas 77204-5003, USA*

\* *Corresponding author; email: vekilov@uh.edu*

### **Abstract**

Crystal morphology plays a pivotal role in all applications because it affects the performance and the processing behaviors of crystals. Foreign compounds are often employed to control crystal morphology; conversely, morphology variations are sometimes attributed to uncontrolled impurities present in the crystallizing solution. Here we explore the impact of modifiers on the crystallization and morphology of mefenamic acid (MFA), a nonsteroidal anti-inflammatory drug. We focus on the roles of benzoic acid, 2-chlorobenzoic acid, and 2,3-dimethylaniline, compounds that may be retained as minor components after MFA synthesis. We explore the effects of these compounds at varying MFA supersaturation levels. Whereas the additives did not alter the polymorphic form of MFA, they significantly modified crystal morphology,

Modifiers regulate crystal morphology by generating lattice defects

leading to elongated and blade-like crystals. In contrast to numerous published cases, these compounds do not affect the growth rates of the dominant crystal faces. Instead, we show that the observed morphology changes are due to modifier-driven crystal twinning that may be initiated by disruptions of crystal nucleation. These findings highlight the importance of considering nonclassical nucleation mechanisms, where impurities and modifiers may influence crystallization through pathways beyond direct surface adsorption, such as cluster formation and lattice disruption. This study provides critical insights into the role of foreign compounds in crystal engineering, emphasizing the need for an integrated outlook on their effects on crystal nucleation and growth to optimize pharmaceutical crystallization strategies and enhance drug performance.

## **Introduction**

The shape and habit are among the critical attributes that determine the properties and applications of all classes of crystals: catalysts,<sup>1-2</sup> of nonlinear optical elements,<sup>3-4, 5</sup> pathological agglomerates,<sup>6-8</sup> and others. Thus, crystal morphology control is a fundamental problem of crystal growth science.<sup>9</sup> Crystal morphology is particularly important for pharmaceutical preparations, for which it dictates the physicochemical properties, processing behaviors, and therapeutic performance of active pharmaceutical ingredients (APIs). Since anisotropic crystal faces dissolve at rates that may vary multifold, the control of crystal shape is essential for optimizing dissolution rates, ensuring bioavailability, and maintaining consistency during drug manufacturing. Among the various morphologies observed in crystalline APIs, blade-shaped (or just blade) crystals present a series of challenges that significantly complicate downstream processing. Their inherent poor flowability disrupts the efficient handling of particulate solids, particularly in continuous manufacturing reactors. The elongated shape of these crystals results in increased interparticle friction and the formation of bridges or clogs in hoppers, feeders, and other material transfer systems.<sup>10</sup> Additionally, the mechanical fragility of blade crystals can result in particle breakage during blending or compression and increasing the heterogeneity of the particle size distribution.<sup>11</sup> Furthermore, inefficient filtration through a tightly packed filter cake created by blade crystals increases the risk of impurity retention, which may affect the overall purity and stability of the API.<sup>12</sup> This ultimately affects batch quality and

## Modifiers regulate crystal morphology by generating lattice defects

compliance with regulatory standards.<sup>13</sup> Post-crystallization modifications, including milling and agglomeration, are often employed to improve particle morphology; these processes, however, may introduce additional complexities. The risk of generating amorphous content or inducing polymorphic transformations during milling is high and may compromise the stability and performance of the API.<sup>14</sup>

Uncontrolled foreign compounds (i.e., distinct from the crystallizing substance and the solvent) are often called impurities and they represent an intrinsic aspect of the crystallization process. They may be introduced along with the raw materials and solvents or created as synthesis byproducts. Even in trace amounts, these foreign molecules may profoundly affect crystal morphology by impeding growth of specific crystal faces.<sup>15-17</sup> Impurities or intentionally introduced modifiers may affect the growth processes on a crystal surface without incorporating into the crystal or, conversely, embed in the crystal lattice without affecting the growth kinetics, both affect growth and incorporate, or do neither.<sup>9</sup> The two primary molecular mechanisms of impurity growth inhibition include kink blocking and step pinning;<sup>18-21</sup> elaborate mechanisms of cooperativity between two or more foreign molecules may lead to synergistic or antagonistic inhibition or straightforward additivity.<sup>20-22</sup> Impurity incorporation often results in macroscopic crystal defects such as dislocations, twinning, inclusions, or pores.<sup>23</sup> More complex impurity-driven scenarios arise from the distinct responses to the presence of foreign compounds of the two main stages of crystallization, nucleation and growth.<sup>24-25</sup> Secondary effects and cooperativity between these processes further confound detailed analyses of impurity effects. For instance, additives that are indifferent to the growth processes may, at longer times, invade the crystal lattice and strain it.<sup>26</sup> The added elastic energy increases the chemical potential of the crystallizing substance in the crystals and lowers the crystallization driving force. Impurity incorporation is face-specific,<sup>1-2</sup> and the resulting slowdown of growth will be face-selective, severely affecting the morphology. Modifiers that do not or only weakly inhibit surface growth may boost the nucleation of nanocrystallites, which get buried into growing crystals, causing elastic strain and potent growth suppression.<sup>22, 27-28</sup> Thus, the effects of foreign compounds on crystallization combine both kinetic and thermodynamic aspects. Somewhat loosely, it is sometimes assumed that during slow growth, thermodynamic factors dominate, allowing the crystal to selectively interact or ignore a modifier.<sup>29 30 31-32</sup> By

Modifiers regulate crystal morphology by generating lattice defects

contrast, it is thought that under fast growth conditions, kinetic factors may dominate, leading to nonlinear response to the impurities.

Current models of crystal morphology control predominantly focus on the suppression of growth in specific directions and have produced significant strides in describing the influence of foreign molecules and solvents on crystal morphology.<sup>33-38</sup> A deeper mechanistic understanding of growth processes and defect formation, particularly in the presence of impurities, is critical for refining these predictive models. Integrating such insights with computational advances would enable more comprehensive and precise control of crystal engineering, allowing for the development of more versatile and reliable crystallization strategies.

Here we report on the crystallization of MFA in the presence of modifiers and examine their effects on the resulting crystal morphology. Mefenamic acid (MFA) is a nonsteroidal anti-inflammatory drug (NSAID) widely used for managing mild to moderate pain, particularly dysmenorrhea (menstrual cramps).<sup>39</sup> Assigned to the Biopharmaceutical Classification System (BCS) Class II, MFA exhibits low solubility but high permeability, making dissolution a rate-limiting step in its bioavailability. MFA exists in three polymorphic forms: I, II, and III, with Form I being the most thermodynamically stable at ambient conditions. Form I enantiotropically relates to Form II, which is more stable above 175 °C.<sup>40</sup> MFA Form I crystallizes into a variety of shapes, ranging from plates to needles, depending on the crystallization conditions such as solvent, supersaturation, and temperature.<sup>41-43</sup> Controlling crystal morphology is therefore crucial for optimizing MFA's therapeutic performance and manufacturability.<sup>44-45</sup>

The sensitivity of MFA morphology to solvents and supersaturation levels makes it a suitable model to investigate the effects of impurities on particle attributes. A previous study of crystallization from 30 different solvents<sup>46</sup> identified several solvents in which the crystal morphology of MFA Form I exhibited a strong dependence on supersaturation. Here we focus on crystallization from one of these solvents, 2-butanol, and explore the effects of three foreign compounds. Two of them, 2-chlorobenzoic acid (ClBA) and 2,3-dimethylaniline (DMA), are the raw materials in MFA manufacture,<sup>47</sup> whereas benzoic acid (BA) is a common byproduct. We combine experimental crystallization studies with adsorption energy calculations

Modifiers regulate crystal morphology by generating lattice defects

to elucidate whether these modifiers impact crystal growth through adsorption on the growing crystal surfaces or via other mechanisms.

## **Materials and Methods**

*Materials.* Analytical grade 2-butanol was purchased from Fisher Scientific, UK. Mefenamic acid ( $\geq 98\%$ ), benzoic acid ( $\geq 99.5\%$ ), 2-Chlorobenzoic acid ( $\geq 98\%$ ), and 2,3-dimethylaniline ( $\geq 99\%$ ) were purchased from Millipore Sigma (formerly Sigma Aldrich) UK and were used without further purification.

*Crystallization of seed crystals:* Plate like crystals grew from 2-butanol at  $C - C_e$  in the range 12 – 19 mM (the solubility of MFA at 25 °C is  $C_e = 23$  mM, Figure S1) and blade-like crystals were grown at  $C - C_e = 22$  mM after a period of 5 – 7 days.

*Growth of crystals.* To measure the growth kinetics of MFA crystals at 20 °C in 2-butanol in the [010] and [001] directions, we used an inverted optical microscope Leica DMi1 equipped with Leica DFC495 camera, Leica Microsystems (UK) Ltd. Images were analyzed using LAS v.4.8 software (Leica). Supersaturated solutions were prepared by dissolving appropriate amounts of MFA at an elevated temperature, after which the solution was slowly cooled down to 20 °C and filtered into a glass vial. The images were collected every 5 min. The growth of each crystal seed was monitored for about 3 h, during which the solution supersaturation was assumed to remain constant as no spontaneous nucleation was observed.

*Solubility measurements.* A known amount of MFA was weighed into a 2 ml vial. 1.5 ml of 2-butanol was pipetted into this pre-weighed vial containing the solid material and a stir bar. The vial was then reweighed to determine the exact mass of solvent added and therefore the exact molar composition of the sample. Each vial was capped tightly to avoid evaporation of the solvent during measurement. The temperature at which all crystals dissolved was measured by a Crystal16 Multiple Reactor (Technobis Crystallization Systems, The Netherlands) using 700 rpm of stirring rate and heating rate 0.2 K/min and was taken as the equilibrium temperature of the tested mixture.

*Face indexing.* Single crystal X-ray diffraction (SC-XRD) patterns was collected using D8 Venture (Bruker UK Limited), equipped with Photon III CCD detector and Cu K $\alpha$  X-ray energy source (1.5406 Å). A single

Modifiers regulate crystal morphology by generating lattice defects

crystal was prepared and fixed onto a low diffraction loop connected to a three-circle fixed Chi goniometer.

The data were collected from 4° to 35° 2-theta (step size 0.017°) at ambient temperature.

*Powder Xray Diffraction:* All samples were analyzed using Bruker AXS D8 Advance II diffractometer using Debye-Scherrer transmission of Cu K $\alpha$ 1 radiation with a wavelength of 1.540596 Å. Samples were prepared on an automated x-y 28 well plate with 7.5  $\mu$ m Kapton film. Patterns were collected between 2 $\Theta$  range 4 – 35°. Reference powder patterns were produced using the Mercury 4.8 (CCDC) software from single-crystal data (CSD ref code: XYANAC).

*Scanning electron microscopy:* Scanning Electron Microscopy images were collected using U9320B 8500B field emission scanning electron microscope (FE-SEM) from Keysight Technologies in backscattered mode at 10kV

*Adsorption energies calculations:* Adsorption energies were modelled using Material Studio 7.0 Software package (Accelrys Software Inc.) Stepped surfaces of each MFA crystal face were created using the Form I crystal structure, CCDC code: XYANAC. First, the unit cell was optimized with Forcite. The Quasi-Newton algorithm was used with convergence tolerance for energy of  $2.0 \times 10^{-5}$  kcal/mol, a force of 0.001 kcal/mol/Å, and the displacement of  $1.0 \times 10^{-5}$  Å. Next, surfaces were created by cleaving the MFA Form I unit cell to a fractional depth of 1 unit cell and constructing a  $3 \times 4$  supercell. Rows of surface molecules were manually deleted to create steps. A vacuum slab of 100 Å was inserted above each surface. The monomer I was cut from MFA Form I (CCDC code: XYANAC) and monomer II was cut from MFA form II (CCDC ref code: XYANAC07). Impurity molecules were drawn in Materials Studio. All geometries were optimized in the same way as described above using Forcite. The COMPASS forcefield was used for the adsorption calculations and rigid monomers were used. Five different adsorption configurations of monomer and dimer were investigated, and the lowest energy configuration is reported. The binding energies calculated using the following equation:  $U_{\text{Ads}} = U_{\text{total}} - (U_{\text{surface}} + U_{\text{Adsorbate}})$ , where  $E_{\text{total}}$  is the total energy of the surface and adsorbate,  $E_{\text{surface}}$  is the energy MFA surface without the adsorbate, and  $E_{\text{adsorbate}}$  is the energy of the adsorbate without the surface.

Modifiers regulate crystal morphology by generating lattice defects

## Results

### *Growth of MFA in pure solution*

The MFA molecule consists of a benzoic acid residue, connected at position 2 by an amino bridge to an ortho-xylene group (Figure 1a). A strong intramolecular hydrogen bond (N–H...O) between the amino and the carboxyl groups keeps the phenyl and carboxyl groups of benzoic acid coplanar with the amino group and leaves a single rotational degree of freedom around the bond between the xylene and amino groups. As a benchmark to quantify modifier effects on MFA crystallization, we conducted crystallization experiments in pure 2-butanol. Crystals obtained from 2-butanol solution of different supersaturation exhibit distinct

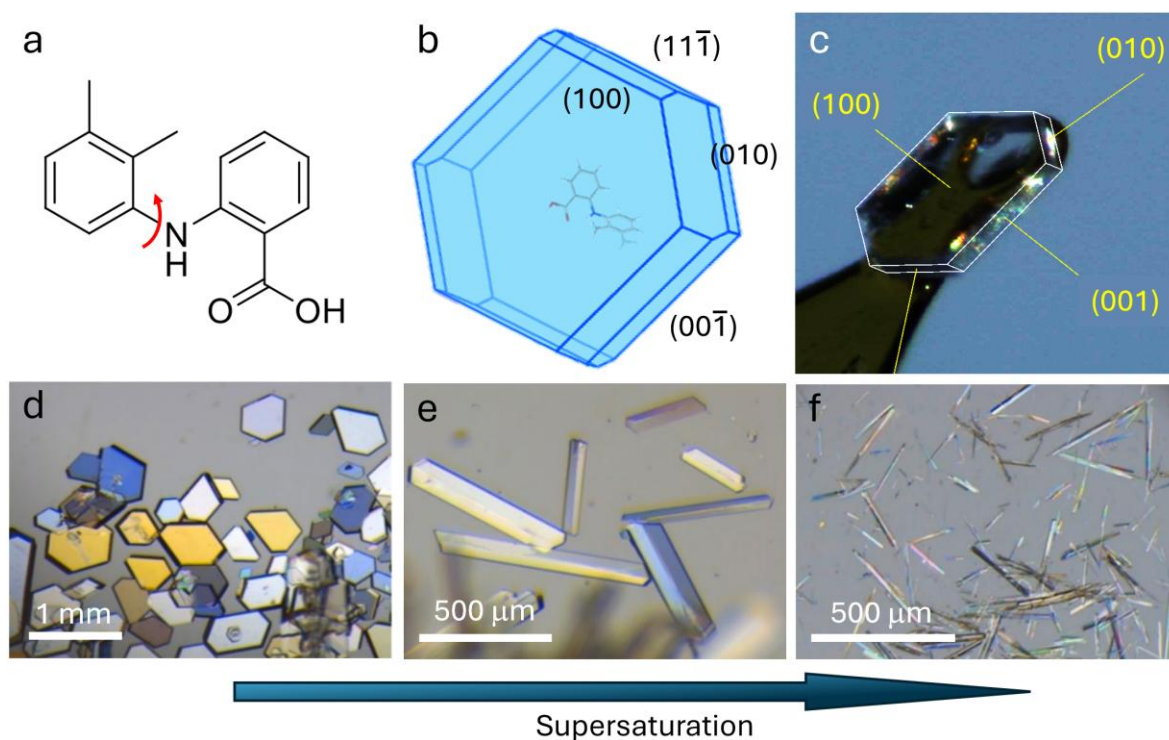


**Figure 1.** Mefenamic acid crystals and their morphology. Form I crystals grown from 2-butanol. a) Molecular structure of MFA. b) BFDH plate crystal morphology generated with Mercury software (version 2021.2.0) using CSD entry XYANAC. c) Face indexing of plate crystals. d) Plate crystals grown at  $C - C_e = 12$  mM. e) Blade-like crystals grown at  $C - C_e = 22$  mM. f) Needle-like crystals grown at  $C - C_e > 25$  mM

morphologies.<sup>46</sup> Despite their morphology differences, all obtained crystals were of the most stable form at ambient conditions, Form I (Figure S2). The Bravais-Friedel-Donnay-Harker (BFDH)<sup>48</sup> model predicts for MFA Form I plate morphology with dominating {100} faces (Figure 1b). This model relies on the generally

## Modifiers regulate crystal morphology by generating lattice defects

accepted rule that faces that grow more slowly are more prominent in the crystal habit<sup>9,49</sup> and evaluates the relative face growth rates solely from the interplanar distances in the respective crystallographic directions. Face indexing using single crystal X-ray diffraction (Figure 1c) confirmed that the experimental plate morphology (Figure 1d) matches the prediction of the BFDH model. As supersaturation increased crystal morphology shifted significantly from that predicted by the model and seen at low supersaturations (Figure 1d). Crystals grown at  $C - C_e = 22$  mM are elongated (Figure 1e); above  $C - C_e = 25$  mM the crystals are even less isometric and present as long and thin needles (Figure 1f).

To understand how supersaturation affects the shape of the crystals during growth, we note that the MFA crystal morphology reflects the anisotropic growth rates of individual crystal faces.<sup>9,49</sup> The size of a crystal face is inversely proportional to its growth rate; slower-growing faces are larger, whereas faster-growing faces are smaller or may taper off into wedges, an implementation of the venerable Chernov rule.<sup>9,49</sup> Thus, concentration-dependent crystal morphologies are a consequence of distinct growth rates – concentration correlations in different crystallographic directions. The crystals grow as solute molecules associate to kinks, located along the steps. The growth rate of a face,  $G$ , can be expressed as a function of the supersaturation ( $C - C_e$ ),  $G = ak_g(C - C_e)^b$ , where  $a$  is the solute molecular size, the exponent  $b$  is the growth order (usually  $1 \leq b \leq 2$ ), and  $k_g$  is the growth constant. We monitored the growth of plate MFA crystals in 2-butanol in  $[01\bar{1}]$  and  $[001]$  directions (Figure 2a) at varying supersaturations expecting to obtain the growth constants in both directions. The measured growth rates appear proportional to the concentration, indicating that the growth order  $b \cong 1$ . The linear  $G(C)$  correlations indicate that the crystals grow by incorporation of the dominant solution species.<sup>50-52</sup> From the slopes of the  $G(C)$  correlations (Figure 2) and the molecular size  $a$  we evaluate the rate constants,  $k_g$ , for incorporation into kinks. The evaluated  $k_g$ s in the  $[001]$  and  $[01\bar{1}]$  directions are similar ( $k_g[001]_{plate} = (1.9 \pm 1.0) \times 10^3 \text{M}^{-1}\text{s}^{-1}$  and  $k_g[01\bar{1}]_{plate} = (2.2 \pm 1.0) \times 10^3 \text{M}^{-1}\text{s}^{-1}$  (Figure 2b, c). The similarity of the measured growth rates in the  $[001]$  and  $[01\bar{1}]$  directions within the probed supersaturation range,  $0 \leq (C - C_e) \leq 0.19$  mM (Figure 2b, c), reflected in the linear  $G(C)$  correlations and the closeness of the respective  $k_g$ s, agrees with the observed isometric plate

Modifiers regulate crystal morphology by generating lattice defects

shape (Figure 2b, c). Extrapolating these linear  $G(C)$  correlations to greater supersaturations, however, contradicts the observed shape transition from plates to blades (Figure 1e, f).

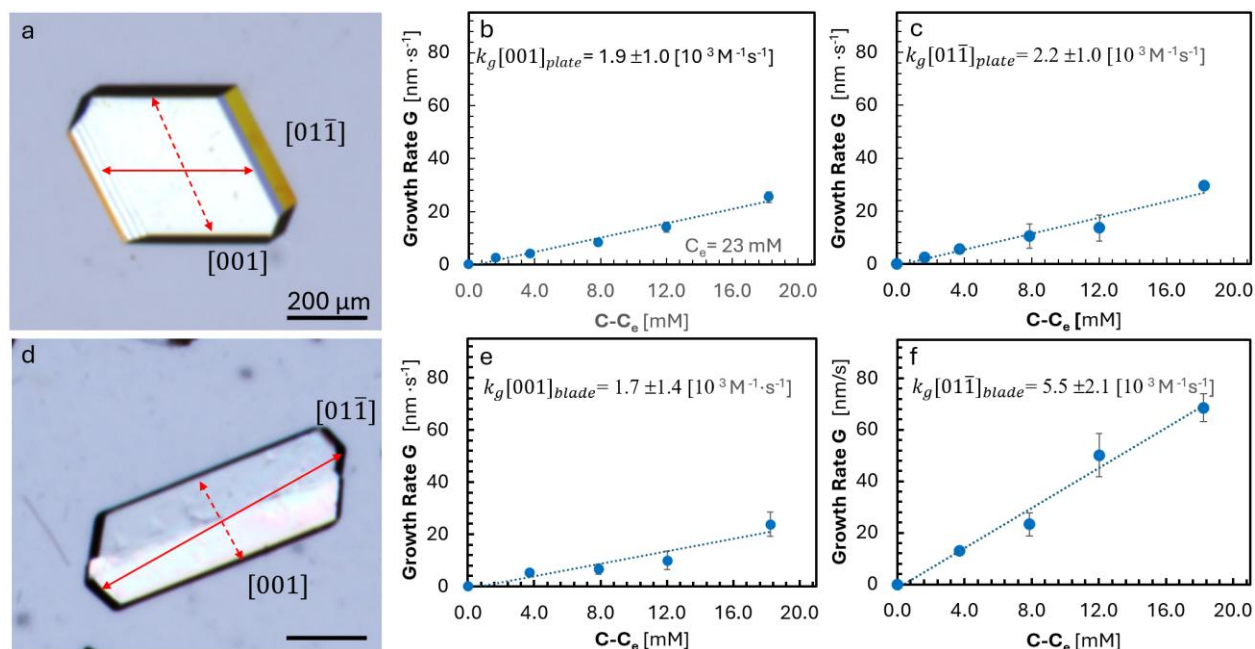


**Figure 2.** Growth kinetics of MFA crystals in the absence of additives. a), d) Micrographs of a plate crystal, in a), and a blade crystal, in d), with denoted crystallographic directions. b), c) Growth rates as functions of the supersaturation  $C - C_e$  in  $[001]$  direction, in b), and in  $[01\bar{1}]$  direction, in c) for plate crystals. e), f) Growth rates as functions of the supersaturation  $C - C_e$  in  $[001]$  direction, in b), and in  $[01\bar{1}]$  direction, in c) for blade crystals. Symbols represent the average values of five independent measurements with different crystals; error bars designate the corresponding standard deviation from these average values. Dotted lines represent best linear fits to data. The growth constants  $k_g$  evaluated as slopes of the dotted lines are shown in the plots.

To understand the inconsistency between the observed blade shape and the prediction based on measurements with plate crystals, we measured the anisotropic growth rates in the  $[01\bar{1}]$  and  $[001]$  directions of blade crystals (Figure 2d). Similarly to the plate crystals the growth rate displayed a linear dependence on concentration. As expected, in contrast to plate crystals, the blade crystals grow significantly faster in the  $[01\bar{1}]$  direction than in the  $[001]$  direction. The growth constant in the  $[001]$  direction,  $k_g[001]_{blade} = 1.7 \pm 1.4 \cdot 10^3 \cdot M^{-1} \cdot s^{-1}$  is similar to that of plate crystals in the same direction, whereas in the  $[01\bar{1}]$  direction, along the blade axis,  $k_g[01\bar{1}]_{blade} = 5.5 \pm 2.0 \cdot 10^3 \cdot M^{-1} \cdot s^{-1}$ , about three-fold higher than that of plate crystals. Notably, the shapes of both plate and blade crystal are preserved across a range of supersaturations. In organic solvents solute reaches the growing steps directly from the solutions, bypassing adsorption on the

Modifiers regulate crystal morphology by generating lattice defects

terraces between steps.<sup>53-54</sup> Thus, the growth rates of the two faces are directly proportional to their respective kink densities. This line of thought leads to the conclusion that the anisotropic growth rates are governed by varying kink densities of different faces and that blade-shaped crystals employ an alternative mechanism to generate more kinks on the  $\{01\bar{1}\}$  faces, which underlies their faster growth.

### *Twinning*

Examinations of blade crystals using optical and scanning electron microscopies reveal that they are twinned (Figure 3). Twinning occurs when two single crystals of the same compound are intergrown along a specific crystallographic plane. A twin boundary separates two domains that are mirror images of each other, creating a symmetric but discontinuous structure.<sup>55-56</sup> This phenomenon typically arises during the early stages of crystallization, around nucleation, at which the crystals are small and the elastic strain associated with the twin boundary is sufficiently low to be overcome by the free energy loss of crystallization.<sup>57-58</sup> The Second Law of thermodynamics dictates that twin boundaries select low-energy lattice planes, which are densely packed and provide a good structural fit between the twin components. In MFA crystals, the twin boundaries orient along the (001) plane (Figure 3a, c).

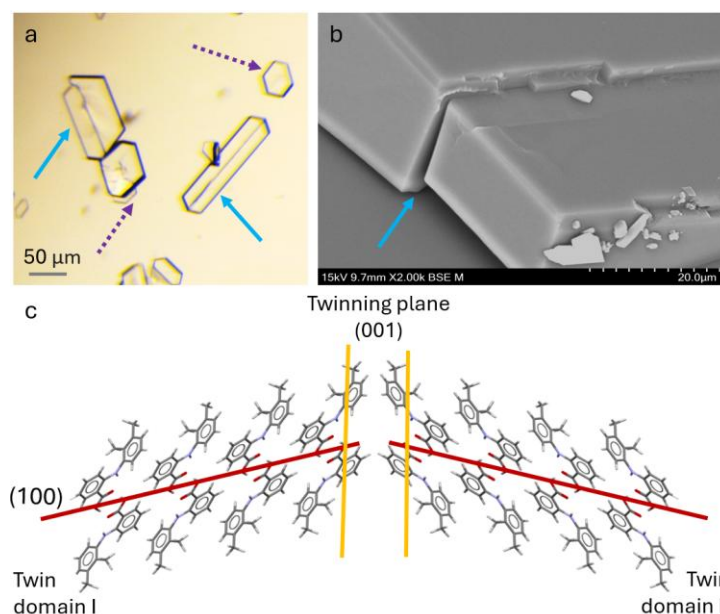


**Figure 3.** Twinning of MFA crystals. a) An optical micrograph of twinned blade crystals marked with solid blue arrows and isometric plate crystals marked with dotted purple arrows. b) A SEM micrograph of a twinned crystal. Blue arrow points at a twin boundary. c) Molecular representation of twinning along a (001) plane.

## Modifiers regulate crystal morphology by generating lattice defects

The effects of twin boundaries on the crystal growth rate have been explored for metal and semiconductor crystals, where these lattice defects are common;<sup>59</sup> the provided mechanistic details appear applicable to organic crystals. The twin boundaries contribute to significantly faster growth by serving as an efficient source of new layers at the re-entrant corners that they create (Figure 3c).<sup>60</sup> The edges of the abundant new layers, the steps, host substantially greater numbers of kinks and lead to faster growth.

### *Growth of MFA in the presence of modifiers*

MFA is synthesized from DMA and ClBA.<sup>47</sup> Common impurities in crude MFA include unreacted DMA and ClBA (Figure 4a). In addition, BA (Figure 4a) is often formed during the reaction, likely due to competing chloride cleavage of ClBA. These impurities are toxic, making their removal by recrystallization crucial.<sup>61-62</sup>

While the presence of modifiers did not alter the solid form (SI Figure 3) their effect on morphology is noticeable. DMA caused moderate elongation and agglomeration of the grown crystals (Figure 4b). By contrast, crystals grown in the presence of ClBA and BA showed strong agglomeration and pronounced elongation in the  $[01\bar{1}]$  direction (Figure 4c, d). The two classical mechanisms of modifier effects on crystal growth rates include step pinning and kink blocking.<sup>19-21, 63-64</sup> Steps may be pinned by modifiers that adsorb directly on the crystal surface and force growing steps to bend if the distance between adsorbed molecules  $\Delta x$  is smaller than the diameter of the critical layer nucleus  $2R_c$  (Figure 4e).<sup>63</sup> Alternatively, the impurities may associate directly to the kink sites and block the access of the incoming solute molecules to this site (Figure 4g). These two mechanisms are identified by variations in the  $G(C)$  correlation that they enforce. Analytical models predicts that steps that are pinned by modifiers do not grow even at solute concentrations that exceed the solubility, leading to a “dead zone” (Figure 4f).<sup>19-20, 63-64</sup> Blocking of kinks suppresses of the growth constant  $k_g$  while preserving the power law  $G(C)$  correlation seen in the absence of a modifier (Figure 4h).<sup>20-21</sup>

Modifiers regulate crystal morphology by generating lattice defects

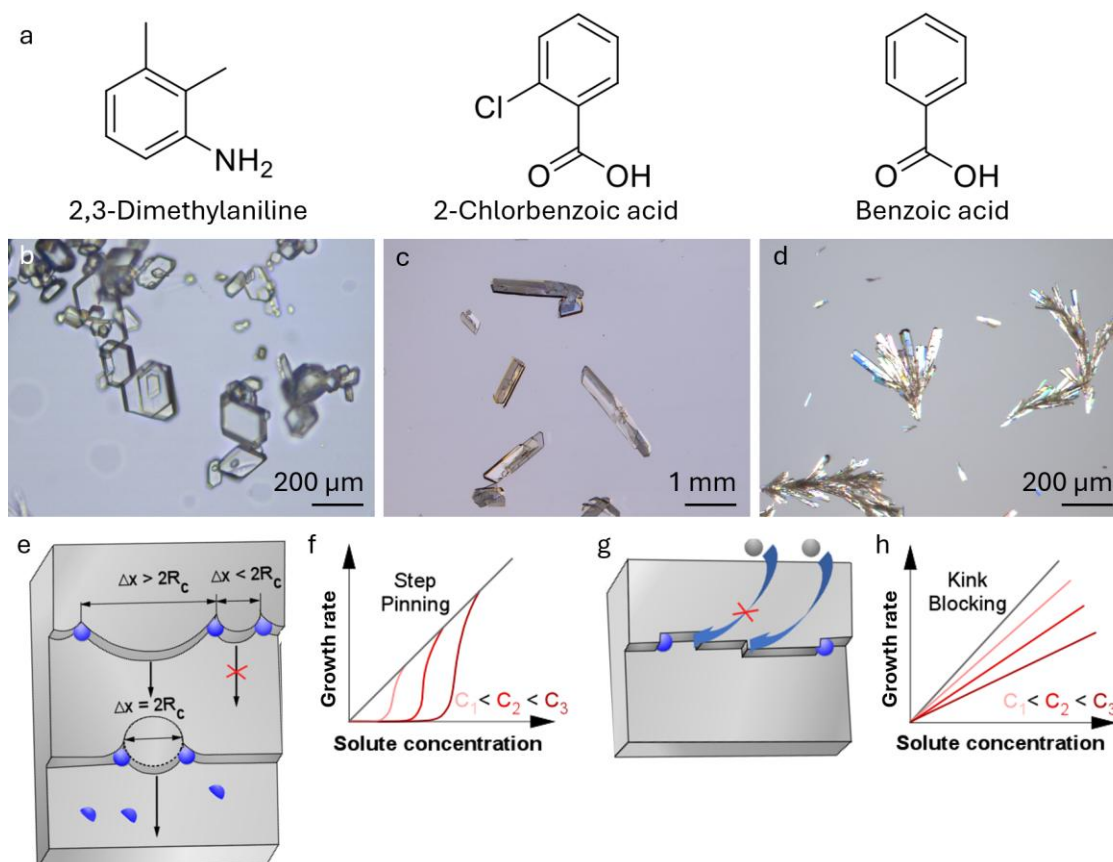


**Figure 4** Effect of modifiers on MFA crystal morphology. a) The molecular structures of DMA, CIBA and BA. b – d) Optical micrographs of MFA crystals grown MFA concentration  $C - C_e = 12$  mM in the presence of 10 mM of b) DME; c) CIBA; and d) BA. e), g) Schematic illustrations of the step pinning, in e), and kink blocking, in g), inhibition mechanisms. f), h) Correlations between the crystal growth rate and solute concentration for the two mechanisms enforced by the presence of modifiers at concentrations increasing in the sequence  $C_1 < C_2 < C_3$ .

We tested whether the mechanisms employed by CIBA and BA to reshape the morphology of MFA crystals involve suppression of the growth in the  $[001]$  direction while leaving the  $\{01\bar{1}\}$  faces free to grow (Figure 5a, b). To discriminate between the two inhibition mechanisms, step pinning and kink blocking (Figure 4e – h) we measured the correlations between the growth rates and MFA concentration for growth in  $[001]$  and  $[01\bar{1}]$  directions of both plate and blade crystals. We chose MFA concentrations in the  $C - C_e$  range from 0 to 19 mM, where, in solutions without additives, the plate shape is preserved during growth (Figure 1d). We chose a constant additive concentrations  $C_{\text{CIBA}} = C_{\text{BA}} = 10$  mM. Contrary to our expectations the tested additives do not change the growth rates of plate crystals in any direction (Figure 5c, d) and of blade crystals in the  $[001]$  direction. The about 15% suppression of the growth

Modifiers regulate crystal morphology by generating lattice defects

rate of blade crystals in the  $[01\bar{1}]$  direction would lead to thicker, not elongated, crystals. The lack of inhibition of the  $\{001\}$  faces indicates that the common mechanism of crystal shape control, through additives that selectively inhibit the growth of specific crystal faces, does not apply to the growth of MFA crystals in presence of ClBA and BA (Figure 5b).

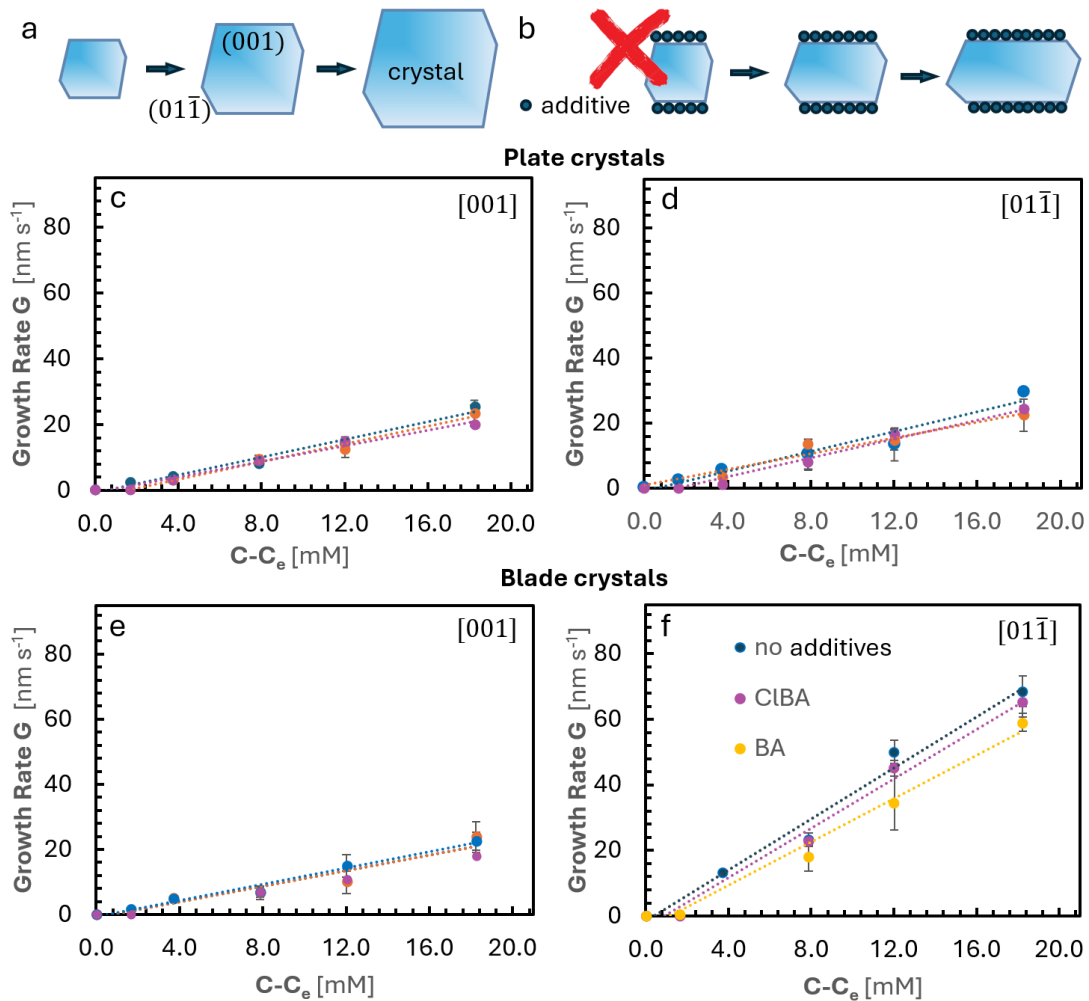


**Figure 5** Effect of modifiers on the growth rates of MFA crystals. a), b) Schematic illustrations of the preservation of the crystal shape during growth from a solution without modifiers, in a), and elongation of crystals in the  $[01\bar{1}]$  direction due to inhibition of the growth of the  $\{001\}$  faces by modifiers, in b). c) – f) Correlations between the crystal growth rate  $G$  and the MFA supersaturation  $C - C_e$  for plate crystals in c) and d) and blade crystals in e) and f) in the presence of 10 mM ClBA or BA, as indicated in legend in f). Growth directions are indicated in the plots. Symbols represent the average values of five independent measurements; error bars designate the corresponding standard deviation from these average values.

Modifiers regulate crystal morphology by generating lattice defects

*The association of modifiers to kinks and terraces is weak*

The nearly complete indifference of ClBA and BA to the growth of the  $\{001\}$  and  $\{01\bar{1}\}$  MFA faces is surprising. The structural similarity of the two modifiers to MFA implies that their interactions with the MFA crystal surfaces would be akin to those of the solute itself, for which attraction with the crystal surfaces represents an essential part of the crystal growth processes. Along this line of thought, we computed the energies of adsorption of DMA, ClBA, and BA to terraces and kinks on several MFA crystal faces (Figure 6a, b). These two surface sites were chosen because modifiers adsorb on the terraces before they pin the steps (Figure 4e) and they associate to kinks to block them (Figure 4g). We compared the adsorption energies of the three modifiers with those of MFA (Figure 6c). To partially account for the conformational variability of MFA, which may assume a line of conformations while in the solution, we use two MFA conformations, belonging to MFA Form I and Form II crystals, respectively. To shorten the computational times, we computed the adsorption energies in vacuum. The biases inherent in this approach partially cancel when we compare the adsorption energies of a modifier and MFA.

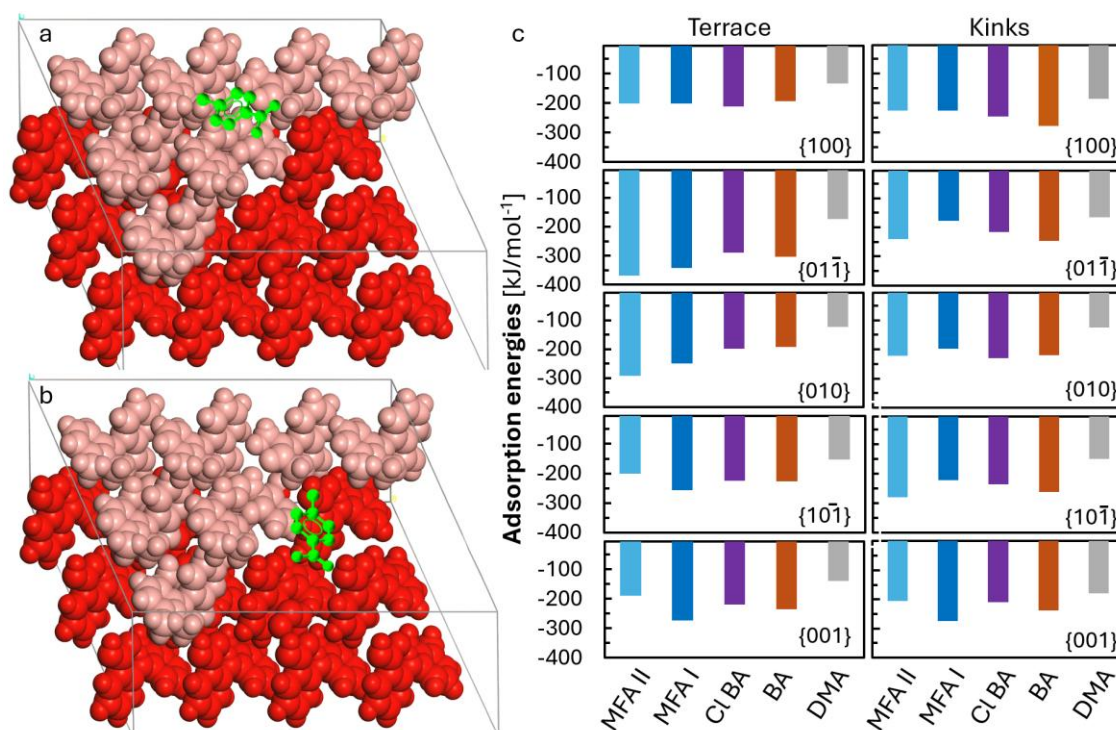


**Figure 6.** Competitive adsorption of ClBA, BA, and DMA on terraces and kinks on five MFA crystal faces. a), b) Schematic representation of the adsorption of an MFA molecule on a crystal terrace, in a), and at a kink, in b). c) Adsorption energies of MFA adopting conformations as in Form II

Modifiers regulate crystal morphology by generating lattice defects

(turquoise) and Form I (blue) crystals and of ClBA (purple), BA (brown) and DMA (Silver) to terraces and kinks on five MFA crystal faces as indicated in the plots.

None of the computed adsorption energies of DMA, ClBA, and BA on surfaces and kinks of the tested crystal faces are significantly lower than those of the two MFA conformers (Figure 6c). Since lower adsorption energy denotes stronger adsorption,<sup>65</sup> this comparison indicates that MFA would likely displace a modifier molecule from any of the probed adsorption sites and not allow it to adsorb. We attribute the appearance of somewhat lower adsorption energies of BA to kinks on the (100) and (01 $\bar{1}$ ) faces than those of the two MFA conformers (Figure 6c) to the inherent biases of the method. This conclusion is supported by the observation that whereas BA appears to slow down weekly the growth of (01 $\bar{1}$ ) faces of blade crystals (Figure 5f), it has no effect on plate crystals (Figure 5d); plate and blade crystals have the same kinks. The inability to adsorb prevents the modifiers from disrupting crystal growth. Unlike scenarios where foreign molecules with strong adsorption can selectively inhibit growth along specific crystallographic directions, leading to morphology modifications, the weak adsorption explains why modifiers do not substantially alter the intrinsic growth characteristics of MFA crystals.

#### *Modifier-induced twinning*

The failure of the mechanism of crystal shape control by modifiers that selectively inhibit specific crystal faces suggests that an alternative mechanism may be behind the observed shape changes in the presence of ClBA and BA (Figure 4c, d). SEM imaging of crystals grown in the presence of the DMA, ClBA, and BA reveal that the latter two modifiers, ClBA and BA, induce substantial twinning in the crystals (Figure 7). Importantly, the twinned crystal grew at MFA concentration  $C - C_e = 12$  mM, within the range where in undoped solutions MFA crystals grow without twinning and retain their isometric hexagonal shapes. The relatively weak adsorption of the modifiers to MFA crystal surface sites suggests that interaction of the modifiers with growing crystals is not how twin boundaries were generated. We tentatively conclude that twinning arises during nucleation and is due to modifiers disrupting the crystal lattice. Thus, even though modifier adsorption is weak, the modifiers still affect crystal evolution by interfering in the nucleation pathways. This

Modifiers regulate crystal morphology by generating lattice defects

distinction is critical in understanding modifier effects in crystal engineering, as it highlights that impurities can impact crystallization outcomes through mechanisms beyond direct surface adsorption.

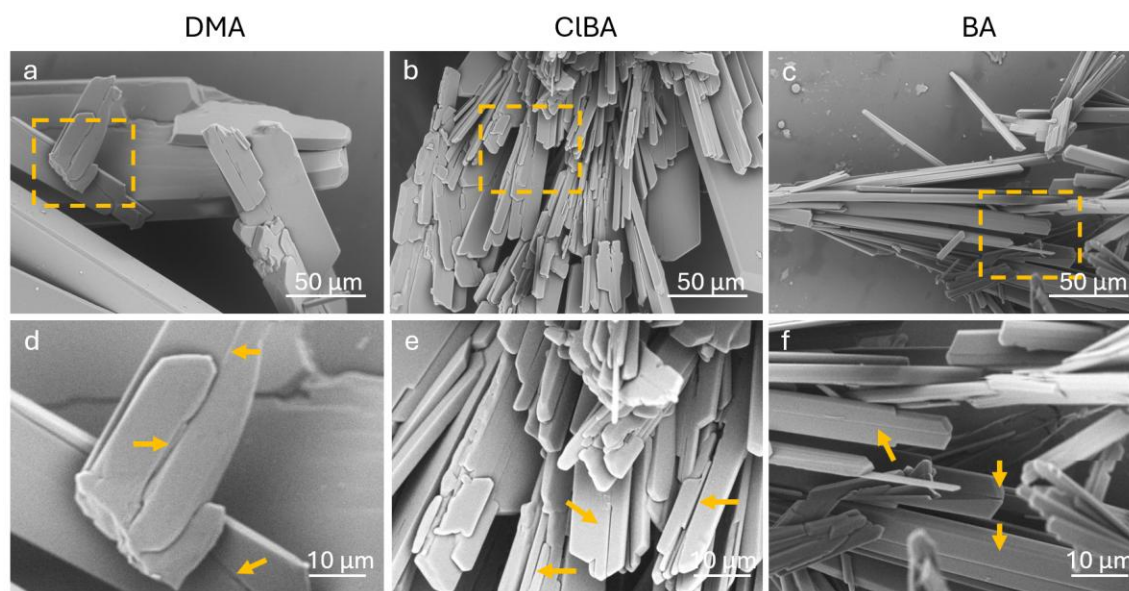


**Figure 7.** Modifier induced twinning of MFA crystals. SEM images of MFA crystals grown at  $C - C_e = 12$  mM and in the presence of 10 mM of DA, in a) and d); CIBA, in b) and e); and BA, in c, and f). Gold contours in a), b) and c) highlight image sections magnified in d), e), and f), respectively. Gold arrows point at twin boundaries.

## Conclusions

We explored the impact of foreign compounds on the crystallization pathways and the resulting morphology variations of MFA. We find that the tested modifiers do not strongly adsorb onto MFA crystal surfaces. As a result, they do not significantly alter the anisotropic growth rates of MFA crystals. Unlike cases where modifier adsorption can selectively hinder crystal growth along specific crystallographic directions, the weak interaction of the tested modifiers with MFA suggests that adsorption-driven modifier-mediated changes in crystal shape are minimal.

Despite the lack of strong adsorption, the presence of modifiers still plays a critical role in shaping the final crystal morphology. The modifiers cause crystal twinning and the engendered twin boundaries serve as sources of new layers, leading to fast growth. The modifiers accomplish this not by directly adsorbing on the crystal surfaces but by disrupting the crystal lattice likely at nucleation, where they may interfere with

Modifiers regulate crystal morphology by generating lattice defects

molecular packing, promoting twin boundary formation. This highlights an essential distinction between modifiers adsorption effects and impurity-driven structural modifications: whereas the former directly influences crystal growth kinetics, the latter contributes to defect formation and crystallographic discontinuities.

Importantly, as non-classical nucleation mechanisms gain increasing recognition in crystallization studies, it is essential to investigate modifiers effects within these frameworks. Many organic and pharmaceutical molecules are now understood to undergo non-classical nucleation, involving the formation of prenucleation clusters, amorphous intermediates, and multi-step pathways before achieving a stable crystalline structure. In this context, foreign compounds may influence crystallization through mechanisms beyond classical adsorption, such as modifying cluster stability, altering intermediate structures, or driving alternative nucleation pathways. Our findings suggest that modifier effects on non-classical nucleation warrant further study, as they may be a key factor in understanding defect formation, polymorphic transformations, and morphological transitions in pharmaceutical crystallization. Addressing these aspects will be crucial for refining crystallization control strategies and optimizing particle attributes for drug development.

## **Associated Content**

### *Supporting Information*

Figure S1. Temperature dependent solubility of MFA I in 2-butanol.

Figure S2. PXRD patterns for MFA.

Figure S3. PXRD patterns for MFA crystals grown in the presence of modifiers.

### *Corresponding Author*

**Peter G. Vekilov** – William A. Brookshire Department of Chemical and Biomolecular Engineering and Welch Center for Advanced Bioactive Materials Crystallization, University of Houston, Houston 77204-4004 Texas, United States; Department of Chemistry, University of

Modifiers regulate crystal morphology by generating lattice defects

Houston, Houston 77204-5003 Texas, United States; [orcid.org/0000-0002-3424-8720](https://orcid.org/0000-0002-3424-8720);  
<https://orcid.org/0000-0002-3424-8720>; Email: [vekilov@uh.edu](mailto:vekilov@uh.edu)

### *Authors*

**Monika Warzecha** – Strathclyde Institute of Pharmacy and Biomedical Sciences, University of Strathclyde, 161 Cathedral Street, Glasgow, G4 0RE, UK, EPSRC Future Continuous Manufacturing and Advanced Crystallization Research Hub, University of Strathclyde, Technology and Innovation Centre, 99 George Street, Glasgow, G1 1RD, U.K. <https://orcid.org/0000-0001-6166-1089>

**Manasa Yerragunta** – William A. Brookshire Department of Chemical and Biomolecular Engineering and Welch Center for Advanced Bioactive Materials Crystallization, University of Houston, Houston 77204-4004 Texas, United States.

**Alastair J. Florence** – Strathclyde Institute of Pharmacy and Biomedical Sciences, University of Strathclyde, 161 Cathedral Street, Glasgow, G4 0RE, UK, EPSRC Future Continuous Manufacturing and Advanced Crystallization Research Hub, University of Strathclyde, Technology and Innovation Centre, 99 George Street, Glasgow, G1 1RD, U.K. <https://orcid.org/0000-0002-9706-8364>

### **Acknowledgements**

We thank Siya Nakapraves for taking optical images of MFA crystals. Funding was provided by the CMAC National Facility, housed within the University of Strathclyde's Technology and Innovation Centre funded with a UKRPIF (UK Research Partnership Investment Fund) capital award (SFC ref H13054) and EPSRC Future Continuous Manufacturing and Advanced Crystallisation Research Hub (Grant Ref:EP/PO06965/1), the National Science Foundation (Awards DMR-2128121), and the Welch Foundation through the Welch Center for Advanced Bioactive Materials Crystallization at the University of Houston, Award V-E-0001, and grant E-2170.

## References

1. Dai, H.; Shen, Y.; Yang, T.; Lee, C.; Fu, D.; Agarwal, A.; Le, T. T.; Tsapatsis, M.; Palmer, J. C.; Weckhuysen, B. M.; Dauenhauer, P. J.; Zou, X.; Rimer, J. D., Finned zeolite catalysts. *Nature Materials* **2020**, *19* (10), 1074-1080.
2. Mallette, A. J.; Seo, S.; Rimer, J. D., Synthesis strategies and design principles for nanosized and hierarchical zeolites. *Nature Synthesis* **2022**, *1* (7), 521-534.
3. De Yoreo, J. J.; Burnham, A. K.; Whitman, P. K., Developing  $\text{KH}_2\text{PO}_4$  and  $\text{KD}_2\text{PO}_4$  crystals for the world's most powerful laser. *International Materials Reviews* **2002**, *47* (3), 113 -- 152.
4. Booth, N. A.; Chernov, A. A.; Vekilov, P. G., Interplay of impurities and solution flow as determinants of step pattern dynamics. *Phys. Rev. E* **2004**, *69*, 011604.
5. Booth, N. A.; Land, T.; Erhmann, P.; Vekilov, P. G., The Aspect Ratio of Potassium Dideuterium Phosphate (DKDP) Crystals. *Crystal Growth & Design* **2004**, *5* (1), 105-110.
6. Rimer, J. D.; An, Z.; Zhu, Z.; Lee, M. H.; Goldfarb, D. S.; Wesson, J. A.; Ward, M. D., Crystal growth inhibitors for the prevention of L-cystine kidney stones through molecular design. *Science* **2010**, *330* (6002), 337-41.
7. Farmanesh, S.; Ramamoorthy, S.; Chung, J.; Asplin, J. R.; Karande, P.; Rimer, J. D., Specificity of Growth Inhibitors and their Cooperative Effects in Calcium Oxalate Monohydrate Crystallization. *Journal of the American Chemical Society* **2014**, *136* (1), 367-376.
8. Chung, J.; Granja, I.; Taylor, M. G.; Mpourmpakis, G.; Asplin, J. R.; Rimer, J. D., Molecular modifiers reveal a mechanism of pathological crystal growth inhibition. *Nature* **2016**, *536*, 446-450.
9. Chernov, A. A., *Modern Crystallography III, Crystal Growth*,. Springer: Berlin, 1984.
10. Chatteraj, S.; Sun, C. C., Crystal and Particle Engineering Strategies for Improving Powder Compression and Flow Properties to Enable Continuous Tablet Manufacturing by Direct Compression. *Journal of Pharmaceutical Sciences* **2018**, *107* (4), 968-974.
11. Feng, Y.; Grant, D. J. W.; Sun, C. C., Influence of crystal structure on the tableting properties of n-alkyl 4-hydroxybenzoate esters (parabens). *Journal of Pharmaceutical Sciences* **2007**, *96* (12), 3324-3333.
12. MacLeod, C. S.; Muller, F. L., On the Fracture of Pharmaceutical Needle-Shaped Crystals during Pressure Filtration: Case Studies and Mechanistic Understanding. *Organic Process Research & Development* **2012**, *16* (3), 425-434.
13. Pilaniya, K.; Chandrawanshi, H. K.; Pilaniya, U.; Manchandani, P.; Jain, P.; Singh, N., Recent trends in the impurity profile of pharmaceuticals. *Journal of advanced pharmaceutical technology & research* **2010**, *1* (3), 302-10.
14. Chikhalia, V.; Forbes, R. T.; Storey, R. A.; Ticehurst, M., The effect of crystal morphology and mill type on milling induced crystal disorder. *European Journal of Pharmaceutical Sciences* **2006**, *27* (1), 19-26.
15. Dandekar, P.; Kuvadia, Z. B.; Doherty, M. F., Engineering Crystal Morphology. **2013**, *43* (Volume 43, 2013), 359-386.

## Modifiers regulate crystal morphology by generating lattice defects

16. McArdle, P.; Erxleben, A., Crystal growth and morphology control of needle-shaped organic crystals. *CrystEngComm* **2024**, *26* (4), 416-430.
17. Hatcher, L. E.; Li, W.; Payne, P.; Benyahia, B.; Rielly, C. D.; Wilson, C. C., Tuning Morphology in Active Pharmaceutical Ingredients: Controlling the Crystal Habit of Lovastatin through Solvent Choice and Non-Size-Matched Polymer Additives. *Crystal Growth & Design* **2020**, *20* (9), 5854-5862.
18. Olafson, K. N.; Ketchum, M. A.; Rimer, J. D.; Vekilov, P. G., Mechanisms of hematin crystallization and inhibition by the antimalarial drug chloroquine. *Proceedings of the National Academy of Sciences* **2015**, *112* (16), 4946-4951.
19. Olafson, K. N.; Nguyen, T. Q.; Rimer, J. D.; Vekilov, P. G., Antimalarials inhibit hematin crystallization by unique drug–surface site interactions. *Proceedings of the National Academy of Sciences* **2017**, *114*, 7531-7536.
20. Ma, W.; Lutsko, J. F.; Rimer, J. D.; Vekilov, P. G., Antagonistic cooperativity between crystal growth modifiers. *Nature* **2020**, *577* (7791), 497-501.
21. Chakrabarti, R.; Vekilov, P. G., Dual Mode of Action of Organic Crystal Growth Inhibitors. *Crystal Growth & Design* **2021**, *21* (12), 7053-7064.
22. Ma, W.; Balta, V. A.; Pan, W.; Rimer, J. D.; Sullivan, D. J.; Vekilov, P. G., Nonclassical mechanisms to irreversibly suppress  $\beta$ -hematin crystal growth. *Communications Biology* **2023**, *6* (1), 783.
23. Chung, J.; Granja, I.; Taylor, M. G.; Mpourmpakis, G.; Asplin, J. R.; Rimer, J. D., Molecular modifiers reveal a mechanism of pathological crystal growth inhibition. *Nature* **2016**, *536* (7617), 446-450.
24. Ma, W.; Verma, L.; Lee, H.-J.; Pan, W.; Sherman, M. B.; Sullivan, D. J.; Rimer, J. D.; Palmer, J. C.; Vekilov, P. G., A nonclassical pathway of  $\beta$ -hematin crystal nucleation enables its suppression by antimalarials. *Communications Chemistry* **2025**, *8*, 246.
25. Lee, H.-J.; Sullivan, D. J.; Rimer, J. D.; Vekilov, P. G., Nonclassical Modes to Inhibit  $\beta$ -Hematin Crystallization. *Advanced Functional Materials* **2025**, e21179.
26. Van de Walle, C. G., Effects of impurities on the lattice parameters of GaN. *Physical Review B* **2003**, *68* (16), 165209.
27. Azargoshasb, H.; Lee, H.-J.; Sullivan, D. J.; Rimer, J. D.; Vekilov, P. G., The Hematin-dihydroartemisinin Adduct Mobilizes a Potent Mechanism to Suppress  $\beta$ -hematin Crystallization. *Journal of Biological Chemistry* **2025**, *301*, 110310.
28. Lee, H.-J.; Massih, S.; Abdullah, M.; Rimer, J. D.; Sullivan, D. J.; Vekilov, P. G., Tafenoquine Disrupts Intraerythrocytic Stages of Malaria Parasites by Inhibiting Nonclassical Pathways of  $\beta$ -Hematin Nucleation and Growth. *Biochemistry* **2025**, *64* (15), 3248–3260.
29. Mukuta, T.; Lee, A. Y.; Kawakami, T.; Myerson, A. S., Influence of Impurities on the Solution-Mediated Phase Transformation of an Active Pharmaceutical Ingredient. *Crystal Growth & Design* **2005**, *5* (4), 1429-1436.
30. Horgan, D. E.; Crowley, L. M.; Stokes, S. P.; Lawrence, S. E.; Moynihan, H. A., Impurity exclusion and retention during crystallisation and recrystallisation-the phenacetin by ethylation of paracetamol process. In *Advanced topics in crystallization*, InTech: 2015.

## Modifiers regulate crystal morphology by generating lattice defects

31. Burel, A.; Couvrat, N.; Tisse, S.; Cartigny, Y.; Cardinael, P.; Coquerel, G. J. T. E. P. J. S. T., Binary phase diagrams between phenanthrene and two of its impurities: 9, 10-dihydroanthracene and carbazole. **2017**, 226 (5), 869-880.
32. Kras, W.; Carletta, A.; Montis, R.; Sullivan, R. A.; Cruz-Cabeza, A. J., Switching polymorph stabilities with impurities provides a thermodynamic route to benzamide form III. *Communications Chemistry* **2021**, 4 (1), 38.
33. Clydesdale, G.; Hammond, R. B.; Ramachandran, V.; Roberts, K. J.; Mougín, P., Molecular Modelling of the Morphology of Organic Crystals in the Presence of Impurity Species: Recent Applications to Naphthalene, Phenanthrene, and Caprolactam Crystals. *Molecular Crystals and Liquid Crystals* **2005**, 440 (1), 235-257.
34. Constance, E. N.; Mohammed, M.; Mojibola, A.; Egiefameh, M.; Daodu, O.; Clement, T.; Ogundolie, T.; Nwawulu, C.; Aslan, K., Effect of Additives on the Crystal Morphology of Amino Acids: A Theoretical and Experimental Study. *The Journal of Physical Chemistry C* **2016**, 120 (27), 14749-14757.
35. Kuvadia, Z. B.; Doherty, M. F., Effect of Structurally Similar Additives on Crystal Habit of Organic Molecular Crystals at Low Supersaturation. *Crystal Growth & Design* **2013**, 13 (4), 1412-1428.
36. Chen, B. D.; Garside, J.; Davey, R. J.; Maginn, S. J.; Matsuoka, M., Growth of m-Chloronitrobenzene Crystals in the Presence of Tailor-Made Additives: Assignment of the Polar Axes from Morphological Calculations. *The Journal of Physical Chemistry* **1994**, 98 (12), 3215-3221.
37. Liu, Y.; Yu, T.; Lai, W.; Ma, Y.; Cao, Y.; Liu, N.; Ge, Z.; Zhao, F., Deciphering Solvent Effect on Crystal Growth of Energetic Materials for Accurate Morphology Prediction. *Crystal Growth & Design* **2020**, 20 (2), 521-524.
38. Schmidt, C.; Ulrich, J., Morphology prediction of crystals grown in the presence of impurities and solvents — An evaluation of the state of the art. *J. Cryst. Growth* **2012**, 353 (1), 168-173.
39. van Eijkeren, M. A.; Christiaens, G. C.; Geuze, H. J.; Haspels, A. A.; Sixma, J. J., Effects of mefenamic acid on menstrual hemostasis in essential menorrhagia. *American journal of obstetrics and gynecology* **1992**, 166 (5), 1419-28.
40. Pang, Y.; Buanz, A.; Telford, R.; Magdysyuk, O. V.; Gaisford, S.; Williams, G. R., A simultaneous X-ray diffraction-differential scanning calorimetry study into the phase transitions of mefenamic acid. *Journal of Applied Crystallography* **2019**, 52 (6), 1264-1270.
41. Panchagnula, R.; Sundaramurthy, P.; Pillai, O.; Agrawal, S.; Raj, Y. A., Solid-state characterization of mefenamic acid. *Journal of Pharmaceutical Sciences* **2004**, 93 (4), 1019-1029.
42. Abdul Mudalip, S. K.; Abu Bakar, M. R.; Jamal, P.; Adam, F.; Che Man, R.; Sulaiman, S. Z.; Mohd Arshad, Z. I.; Md. Shaarani, S., Effects of Solvents on Polymorphism and Shape of Mefenamic Acid Crystals. *MATEC Web of Conferences* **2018**, 150, 02004.
43. Assaf, S.; Khanfar, M.; Obeidat, R.; Arida, A., Effect of Different Organic Solvents on Crystal Habit of Mefenamic Acid. *Jordan Journal of Pharmaceutical Sciences* **2009**, 2, 150-157.

## Modifiers regulate crystal morphology by generating lattice defects

44. Prasad, E.; Robertson, J.; Halbert, G. W., Mefenamic acid solid dispersions: Impact of formulation composition on processing parameters, product properties and performance. *Int J Pharm* **2022**, *616*, 121505.
45. Prasad, E.; Robertson, J.; Halbert, G. W., Improving Consistency for a Mefenamic Acid Immediate Release Formulation. *Journal of Pharmaceutical Sciences* **2020**, *109* (11), 3462-3470.
46. Nakapraves, S.; Warzecha, M.; Mustoe, C. L.; Srirambhatla, V.; Florence, A. J., Prediction of Mefenamic Acid Crystal Shape by Random Forest Classification. *Pharmaceutical Research* **2022**, *39* (12), 3099-3111.
47. Trinus, F. P.; Mokhort, N. A.; Yagupol'skii, L. M.; Fadeicheva, A. G.; Danilenko, V. S.; Ryabukha, T. K.; Fialkov, Y. A.; Kirichek, L. M.; Endel'man, É. S.; Get'man, G. A., Mefenamic acid — A nonsteroid antiinflammatory agent. *Pharmaceutical Chemistry Journal* **1977**, *11* (12), 1706-1711.
48. Donnay, J. D. H.; Harker, D., A new law of crystal morphology extending the Law of Bravais. *American Mineralogist* **1937**, *22* (5), 446-467.
49. Chernov, A. A., The spiral growth of crystals. *Sov. Phys. Uspekhi* **1961**, *4*, 116-148.
50. Warzecha, M.; Verma, L.; Johnston, B. F.; Palmer, J. C.; Florence, A. J.; Vekilov, P. G., Olanzapine crystal symmetry originates in preformed centrosymmetric solute dimers. *Nature Chemistry* **2020**, *12* (10), 914-920.
51. Verma, L.; Warzecha, M.; Chakrabarti, R.; Hadjiev, V. G.; Palmer, J. C.; Vekilov, P. G., How to Identify the Crystal Growth Unit. *Israel Journal of Chemistry* **2021**, *61*, 1-11.
52. Warzecha, M.; Verma, L.; Chakrabarti, R.; Hadjiev, V. G.; Florence, A. J.; Palmer, J. C.; Vekilov, P. G., Precrystallization solute assemblies and crystal symmetry. *Faraday Discussions* **2022**, *235* (0), 307-321.
53. Vekilov, P. G.; Verma, L.; Palmer, J. C.; Chakrabarti, R.; Warzecha, M., The pathway from the solution to the steps. *J. Cryst. Growth* **2022**, *599*, 126870.
54. Yerragunta, M.; Tiwari, A.; Chakrabarti, R.; Rimer, J. D.; Kahr, B.; Vekilov, P. G., A dual growth mode unique for organic crystals relies on mesoscopic liquid precursors. *Communications Chemistry* **2024**, *7* (1), 190.
55. De Rosa, C.; Auriemma, F., *Crystals and crystallinity in polymers: diffraction analysis of ordered and disordered crystals*. John Wiley & Sons: 2013.
56. Dhanaraj, G.; Byrappa, K.; Prasad, V.; Dudley, M. J. S. H. o. C. G., Crystal growth techniques and characterization: an overview. **2010**, 3-16.
57. Li, K.; Gbabode, G.; Sanselme, M.; Nicolaï, B.; Guiblin, N.; Rietveld, I. B., Relation between Twinning and Disorder in the  $\gamma$  Form of Pyrazinamide. *Crystal Growth & Design* **2023**, *23* (4), 2463-2469.
58. Hirth, J. P.; Wang, J.; Tomé, C. N., Disconnections and other defects associated with twin interfaces. *Progress in Materials Science* **2016**, *83*, 417-471.
59. Wang, J.; Beyerlein, I. J.; Hirth, J. P.; Tomé, C. N., Twinning dislocations on  $\{1\bar{0}11\}$  and  $\{1\bar{0}13\}$  planes in hexagonal close-packed crystals. *Acta Materialia* **2011**, *59* (10), 3990-4001.
60. Kutsukake, K.; Abe, T.; Usami, N.; Fujiwara, K.; Morishita, K.; Nakajima, K., Formation mechanism of twin boundaries during crystal growth of silicon. *Scripta Materialia* **2011**, *65* (6), 556-559.

Modifiers regulate crystal morphology by generating lattice defects

61. Morcoss, M. M.; Abdelwahab, N. S.; Ali, N. W.; Elsaady, M. T., Different Chromatographic Methods for Simultaneous Determination of Mefenamic Acid and Two of Its Toxic Impurities. *Journal of Chromatographic Science* **2017**, 55 (7), 766-772.
62. Morcoss, M. M.; Abdelwahab, N. S.; Ali, N. W.; Elsaady, M. T., Different Spectrophotometric Methods for Determination of Mefenamic Acid in Presence of its Two Toxic Impurities. *Analytical Chemistry Letters* **2016**, 6 (4), 398-407.
63. Cabrera, N.; Vermilyea, D. A., The growth of crystals from solution. In *Growth and Perfection of Crystals*, Doremus, R. H.; Roberts, B. W.; Turnbull, D., Eds. Wiley: New York, 1958; Vol. 393-408.
64. De Yoreo, J. J., Physical Mechanisms of Crystal Growth Modification by Biomolecules. *AIP Conference Proceedings* **2010**, 1270 (1), 45-58.
65. Liang, Z.; Chen, J.-F.; Ma, Y.; Wang, W.; Han, X.; Xue, C.; Zhao, H. J. C., Qualitative rationalization of the crystal growth morphology of benzoic acid controlled using solvents. **2014**, 16 (27), 5997-6002.

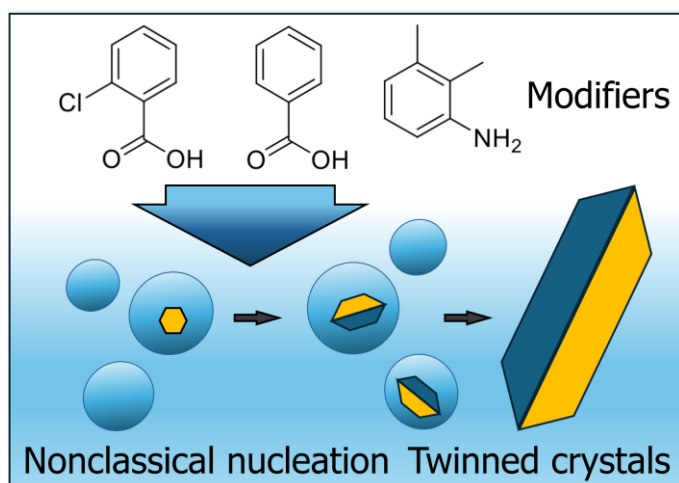
Modifiers regulate crystal morphology by generating lattice defects

## For Table of Contents Use Only

## Modifiers regulate crystal morphology by generating lattice defects

Monika Warzecha, Manasa Yerragunta, Alastair J. Florence, Peter G. Vekilov

### TOC Graphic



### Synopsis

Modifiers can strongly reshape crystal morphology without inhibiting face-specific growth. Using mefenamic acid as a model system, this study shows that structurally related impurities do not alter growth kinetics via adsorption but instead induce crystal twinning, likely during nucleation. The resulting twin boundaries accelerate anisotropic growth, yielding elongated crystals and highlighting nonclassical, defect-mediated pathways of morphology control.

Modifiers regulate crystal morphology by generating lattice defects

## **Supporting Information for**

### **Modifiers regulate crystal morphology by generating lattice defects**

Monika Warzecha,<sup>1,2</sup> Manasa Yerragunta,<sup>3,4</sup> Alistair Florence,<sup>1,2</sup> Peter G. Vekilov<sup>3,4,5,\*</sup>

<sup>1</sup> *Strathclyde Institute of Pharmacy and Biomedical Sciences, University of Strathclyde, 161 Cathedral Street, Glasgow, G4 0RE, UK*

<sup>2</sup> *EPSRC Future Continuous Manufacturing and Advanced Crystallization Research Hub, University of Strathclyde, Technology and Innovation Centre, 99 George Street, Glasgow, G1 1RD, U.K.*

<sup>3</sup> *William A. Brookshire Department of Chemical and Biomolecular Engineering, 4226 Martin L. King Blvd., University of Houston, Houston, Texas 77204-4004, USA*

<sup>4</sup> *Welch Center for Advanced Bioactive Materials Crystallization, University of Houston, 4226 Martin L. King Blvd., Houston, Texas 77204-4004, USA*

<sup>5</sup> *Department of Chemistry, University of Houston, 3585 Cullen Blvd., Houston, Texas 77204-5003, USA*

\* *Corresponding author; email: vekilov@uh.edu*

Modifiers regulate crystal morphology by generating lattice defects

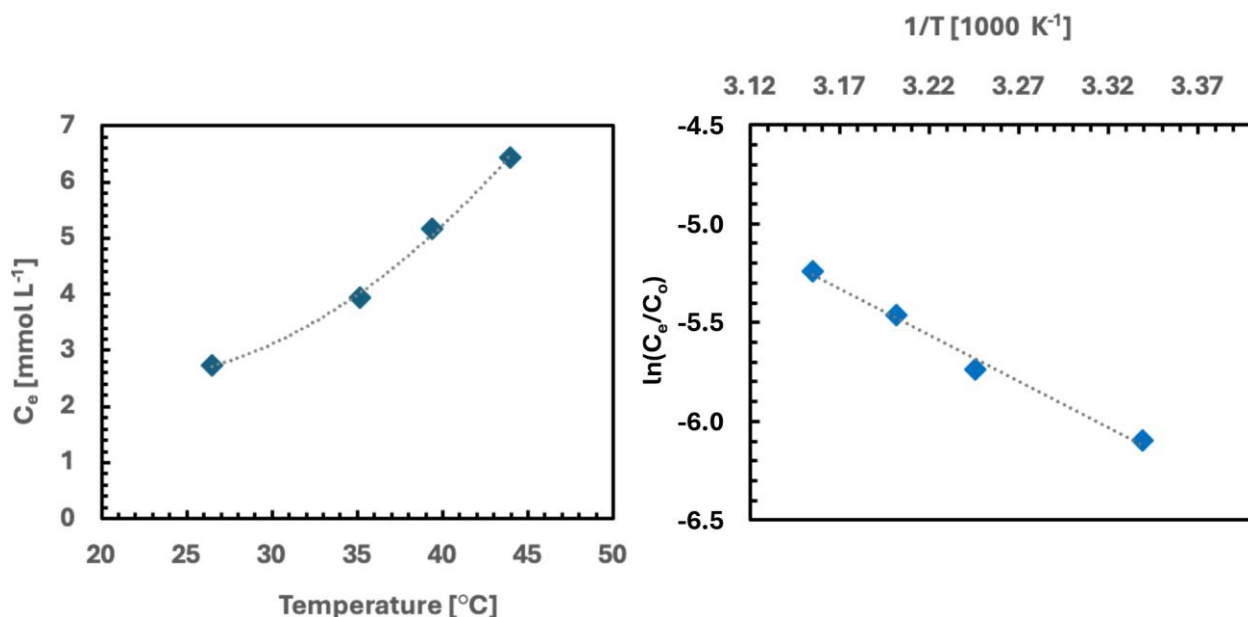


**Figure S6.** a) The temperature dependence of the solubility of MFA Form I crystals in 2-butanol. b) The solubility data in van 't Hoff coordinates.

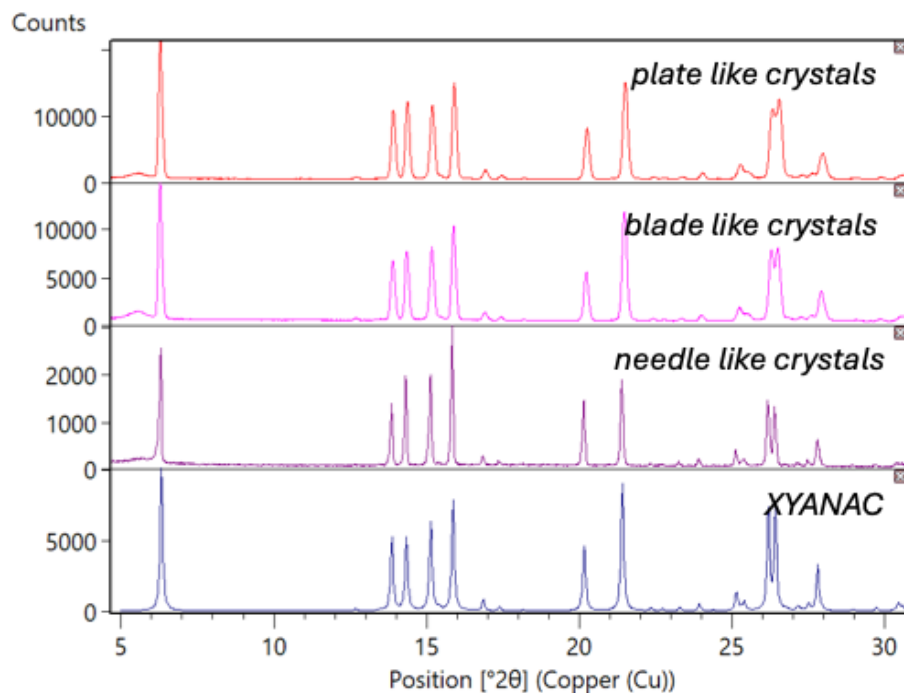


**Figure S7.** Powder x-ray diffraction (PXRD) patterns of MFA crystals. a) Plate-like crystals grown at  $C-C_e = 12-19 \text{ mM}$ . b) Blade-like crystals grown at  $C-C_e = 22 \text{ mM}$ . c) Needle like crystals grown at  $C-C_e > 25 \text{ mM}$ . d) PXRD pattern modelled using Mercury for MFA Form I crystal structure CSD ref code XYANAC.

Modifiers regulate crystal morphology by generating lattice defects

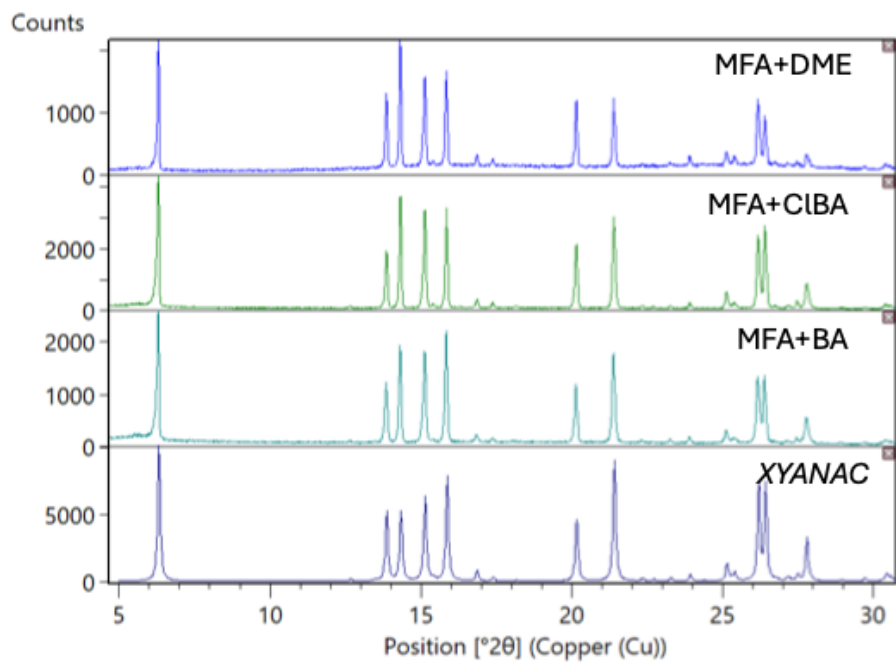


**Figure S8.** PXRD patterns of MFA crystals grown in the presence of modifiers. a) DME, b) CIBA, c) BA, d) PXRD pattern modelled using Mercury for MFA Form I crystal structure CSD ref code XYANAC.